AGU ADVANCING EARTH AND SPACE SCIENCES

Geophysical Research Letters®

RESEARCH LETTER
10.1029/2023GL107385

Key Points:

- We present a novel data set of cosmogenic paleothermometry and luminescence photochronometry at the Gotthard Pass, Switzerland
- Stable Holocene environmental conditions are followed by increases in ground temperature and insolation caused by snow cover decline
- These environmental changes began between 1504 and 1807 CE, tying the observed snowpack decline with the onset of human industrialization

Supporting Information:

Supporting Information may be found in the online version of this article.

Correspondence to:

B. Guralnik and M. M. Tremblay,
benny.guralnik@gmail.com;
tremblam@purdue.edu

Citation:

Guralnik, B., Tremblay, M. M., Phillips, M., Sellwood, E. L., Gribenski, N., Presl, R., et al. (2024). Three centuries of snowpack decline at an Alpine pass revealed by cosmogenic paleothermometry and luminescence photochronometry. *Geophysical Research Letters*, *51*, e2023GL107385. https://doi.org/10.1029/2023GL107385

Received 17 NOV 2023
Accepted 8 JAN 2024

Three Centuries of Snowpack Decline at an Alpine Pass Revealed by Cosmogenic Paleothermometry and Luminescence Photochronometry

Benny Guralnik[1,2], Marissa M. Tremblay[3], Marcia Phillips[4,5], Elaine L. Sellwood[1,2], Natacha Gribenski[6,7], Robert Presl[8], Anna Haberkorn[4], Reza Sohbati[2], David L. Shuster[9,10], Pierre G. Valla[11], Mayank Jain[2], Konrad Schindler[8], Jakob Wallinga[1], and Kristina Hippe[12]

[1]Soil Geography & Landscape Group and Netherlands Centre for Luminescence Dating, Wageningen University, Wageningen, The Netherlands, [2]DTU Physics, Technical University of Denmark, Roskilde, Denmark, [3]Department of Earth, Atmospheric, and Planetary Sciences, Purdue University, West Lafayette, IN, USA, [4]WSL Institute for Snow and Avalanche Research SLF, Davos Dorf, Switzerland, [5]Climate Change, Extremes and Natural Hazards in Alpine Regions Research Centre CERC, Davos Dorf, Switzerland, [6]Institute of Geological Sciences, University of Bern, Bern, Switzerland, [7]Oeschger Centre for Climate Change Research, University of Bern, Bern, Switzerland, [8]Institute of Geodesy and Photogrammetry, ETH Zürich, Zürich, Switzerland, [9]Department of Earth and Planetary Science, University of California, Berkeley, CA, USA, [10]Berkeley Geochronology Center, Berkeley, CA, USA, [11]University Grenoble Alpes, University Savoie Mont Blanc, CNRS, IRD, IFSTTAR, ISTerre, Grenoble, France, [12]Laboratory of Ion Beam Physics, ETH Zürich, Zürich, Switzerland

Abstract The spatial and temporal distribution of Alpine snow is a sensitive gauge of environmental change. While understanding past snow dynamics is essential for reconstructing past climate and forecasting future trends, reliable snowpack data prior to the instrumental record are scarce. We present a novel pairing of cosmogenic paleothermometry and luminescence photochronometry which constrain the temperature and insolation history of bedrock outcrops at the Gotthard Pass, Switzerland, over the last ∼15,000 years. By coupling these results with cosmogenic ^{14}C-^{10}Be chronology and modern in situ rock thermometry, we infer a ∼70-day reduction of snowpack at the topographic mid-slope. Our data indicate stable environmental conditions throughout the Holocene, followed by a 6.6 ± 2.9°C increase of ground surface temperature, coeval with an order-of-magnitude or more increase in ground surface insolation. Bracketing the onset of these changes between 1504 and 1807 CE, our findings tie the snowpack decline with the onset of human industrialization.

Plain Language Summary The extent of snow cover is shrinking in high elevation mountain environments due to climate change. However, it is challenging to determine when snow cover began to change because humans have only been monitoring snow cover for several decades, and snow cover has appeared to shrink over this entire time. We used two new geologic records of ground temperature and light exposure—both of which are impacted by the duration and amount of snow cover—to assess when snow cover began to change in the Gotthard Pass in Switzerland. We found that the middle slopes of the pass began experiencing snow cover loss three centuries ago, well before historical monitoring of snow cover in this region. This record of prolonged snow cover loss matters for the informed management of mountain water sources, rock and snow avalanche risk, and ecosystem change.

1. Introduction

In high elevation mountain environments, snowpack plays a key role in determining ground temperature (Haberkorn et al., 2021) due to its physical characteristics (Arenson et al., 2021) and prolonged duration (Bender et al., 2020). Beyond modulating the ground surface temperature (GST), Alpine snow is also a critical water resource (Brunner et al., 2023), a limiting factor for soil microbial activity (Rindt et al., 2023), and one of the key drivers of topographic slope instability (Cicoira et al., 2019; Kenner et al., 2020). While the ongoing changes in Alpine snowpack due to climate change are well-documented (Buchmann et al., 2021; Klein et al., 2016), they are difficult to evaluate prior to the instrumental record. In the European Alps, snow monitoring data has demonstrated a systematic decline in the duration and height of snowpack from the 1970s and onwards, irrespective of region or elevation (Klein et al., 2016). While the onset and trend in measured snowpack decline correlate inversely with the rise in global temperatures, we lack knowledge on when precisely this decline started. A major reason for this gap is because temperature is only one of many factors influencing the duration of seasonal

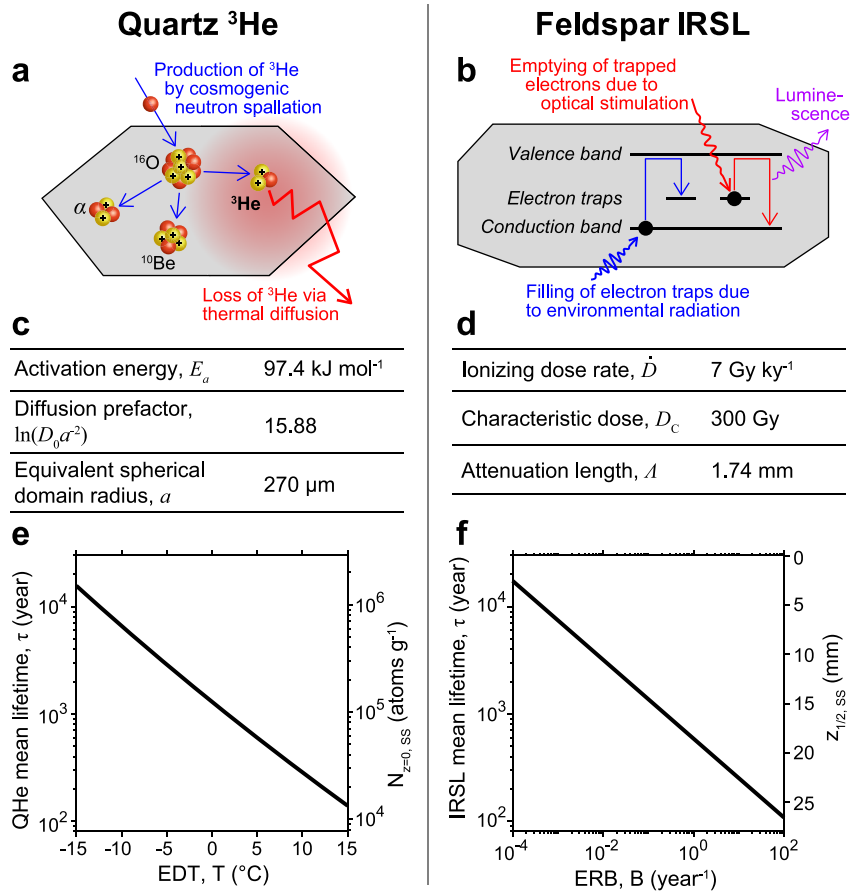

Figure 1. Comparison of QHe (a, c, e) and IRSL (b, d, f) in terms of primary physical drivers (a, b), representative kinetics (c, d), and mean lifetimes and sensitivities (e, f). (a, b) Pathways of concentration accumulation (blue) and loss (red). (c, d) Representative (got-11) kinetic parameters of the QHe (c) and IRSL (d) systems, used to calculate mean lifetimes in (e, f). (e) Effective Diffusion Temperature (EDT) modulates the mean lifetime of QHe, τ (left y-axis), defined as the time taken to reach $1 - e^{-1}$ (~68%) of the maximum attainable concentration (right y-axis) at that temperature. f, Effective Rate of Bleaching (ERB) modulates the mean lifetime of IRSL, τ (left y-axis), defined as the time taken for the inflection point of the concentration-depth profile to progress to $1 - e^{-1}$(~68%) of its deepest attainable depth (right y-axis).

snowpack; other key factors include local terrain, precipitation, orographic effects, wind regime, and ground surface characteristics (Mott et al., 2014). In high-elevation Alpine environments with complex microtopography, a patchwork of snow-covered and snow-free areas can coexist on spatial scales as small as 10^0–10^2 m. Thus, in order to be able to quantify patterns of snow cover prior to the instrumental record, the paleoclimate community needs paleo-snow proxies (Li et al., 2019; Watanabe et al., 2021; Woodhouse, 2003) that (a) have a causal physical relation to snowpack characteristics, (b) have a spatial sensitivity commensurate with the spatial variability of snowpack, and (c) are capable of recording past events over geological timescales of interest.

In this work, we reconstruct a continuous ~15,000-year long snowpack evolution at the Gotthard Pass, Switzerland, through a novel pairing of two Quaternary dating techniques: cosmogenic paleothermometry using ^{3}He in quartz (QHe; Figure 1a), and luminescence photochronometry using infrared stimulated luminescence in feldspar (IRSL; Figure 1b). Both QHe and IRSL are products of high-energy particle fluxes of galactic and terrestrial origin, respectively (Sohbati, Jain, & Murray, 2012; Tremblay et al., 2014a). Production of QHe occurs mainly through nuclear spallation of lattice atoms by secondary cosmic ray neutrons, and its loss is driven by thermal diffusion $\partial n/\partial t = -D_0 a^{-2} e^{-E_a/RT} \nabla^2 n$ (Figure 1c), where T is temperature and the corresponding mean lifetime at that temperature is $\tau \approx \ln(\pi)/\left(15\, D_0 a^{-2} e^{-E_a/\mathrm{RT}}\right)$. The production of trapped electrons giving rise to IRSL occurs via lattice ionisation due to environmental radiation; their photo-stimulated release obeys $\partial n/\partial t = -Be^{-z/\Lambda}n$, where B is a surficial bleaching rate, and z is depth (Figure 1d). A reference depth where half the traps are filled at steady-state ($z_{1/2,SS}$) has an associated lifetime $\tau \approx \ln(2)\, B^{-\exp(-1)} \left(\dot{D}/D_C\right)^{\exp(-1)-1}$. Considering the high

10.1029/2023GL107385

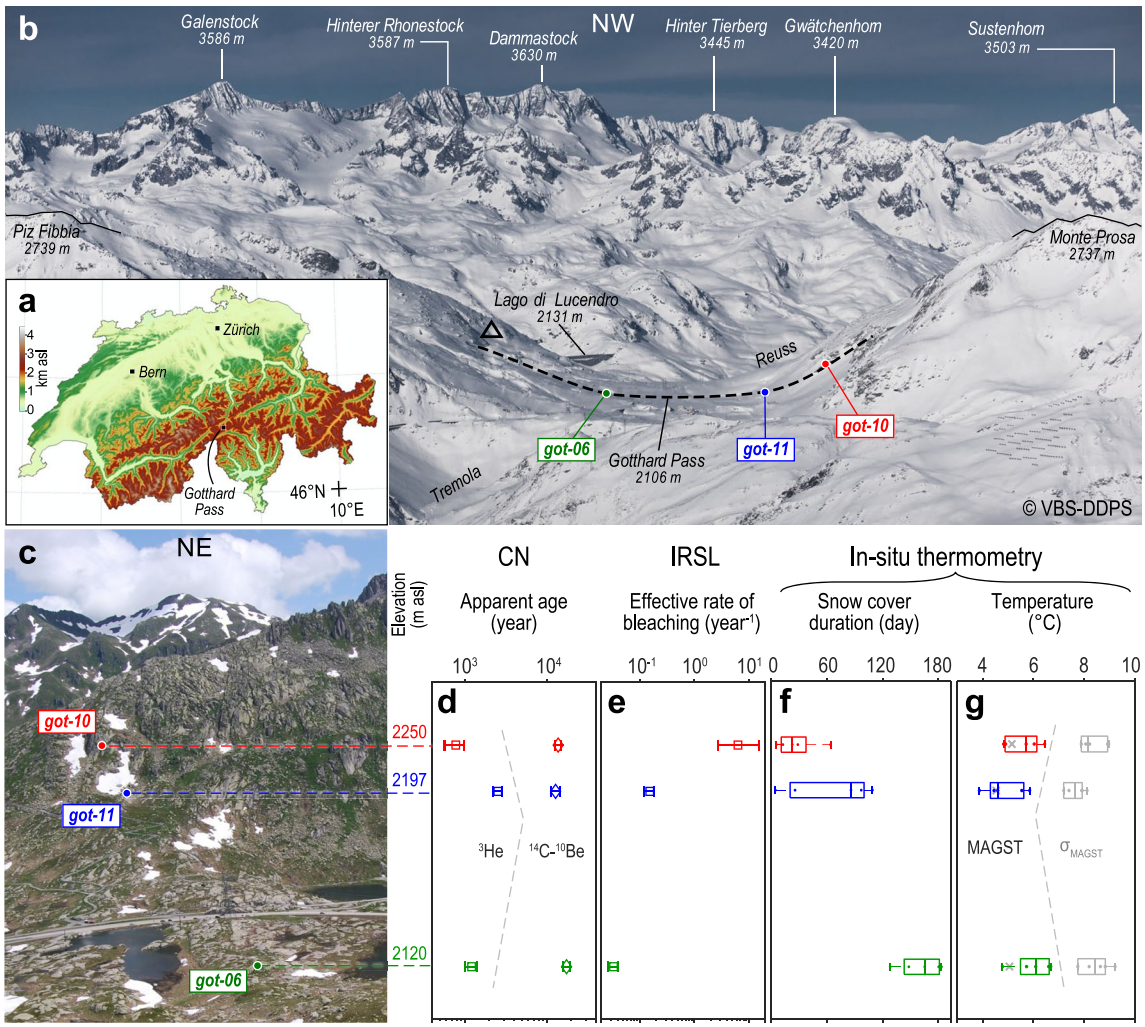

Figure 2. Study site and overview of key results. (a) Topographic map of Switzerland with location of Gotthard Pass. (b) Aerial photograph of the Gotthard pass in February 2012 indicating key landmarks, the pass transect from Hippe et al. (2014) (dashed black line), and sites got-06 (green), got-11 (blue) and got-10 (red). Note that this color scheme is persistent throughout the paper and the Supporting Information S1. (c) Study sites (as viewed from a location marked with a triangle in b), during October 2010 (d) Apparent exposure ages of quartz ^{3}He (squares) and the quartz ^{10}Be-^{14}C isochron from Hippe et al. (2014) (diamonds). (e) Feldspar IRSL effective rates of bleaching. (f, g) Modern in-situ thermometry (2016–2022), including calculated snowpack duration (f), and the annual ground surface temperature, expressed in both in terms of its mean (MAGST) and its 1 standard deviation (σ_{MAGST}) (g).

sensitivity of QHe to temperature ($\partial\tau/\partial T \sim 16\%\ °C^{-1}$; Figure 1e), and of IRSL to bleaching rate ($\partial\tau/\partial B = -0.37\tau/B$; Figure 1f), we may expect to resolve >1°C changes in temperature, and >50% in insolation rate, if these have occurred within the past ~10^2–10^4 years.

The Gotthard Pass (Figures 2a–2c) is a high-elevation (2200–2400 m asl) watershed of the Alpine complex (Davies & Phillips, 1985), characterized by high precipitation (2,400 mm year^{-1}) and low mean annual air temperatures (−1°C) (Ambühl, 1990). Pervasive glacial scour marks at the macroscale, and ice polish at the microscale, as preserved in the barren granitic landscape surrounding the pass, attest to its prolonged submersion under the European Ice Cap until 16–12 ky ago, as determined by a detailed cosmogenic ^{14}C-^{10}Be chronology (Hippe et al., 2014). Since then, the topography is believed to have been ice-free, with only seasonal snow coverage (<3 m during 6 months per year on average) suggested by the ^{14}C-^{10}Be systematics (Hippe et al., 2014). In this work, we selected three representative sites previously dated with ^{14}C-^{10}Be (Figures 2b and 2c); these include the topographic saddle (got-06), a down-valley limit (buttress) of a mid-slope glacial cirque (got-11), and a steep rock wall of the U-shaped valley (got-10).

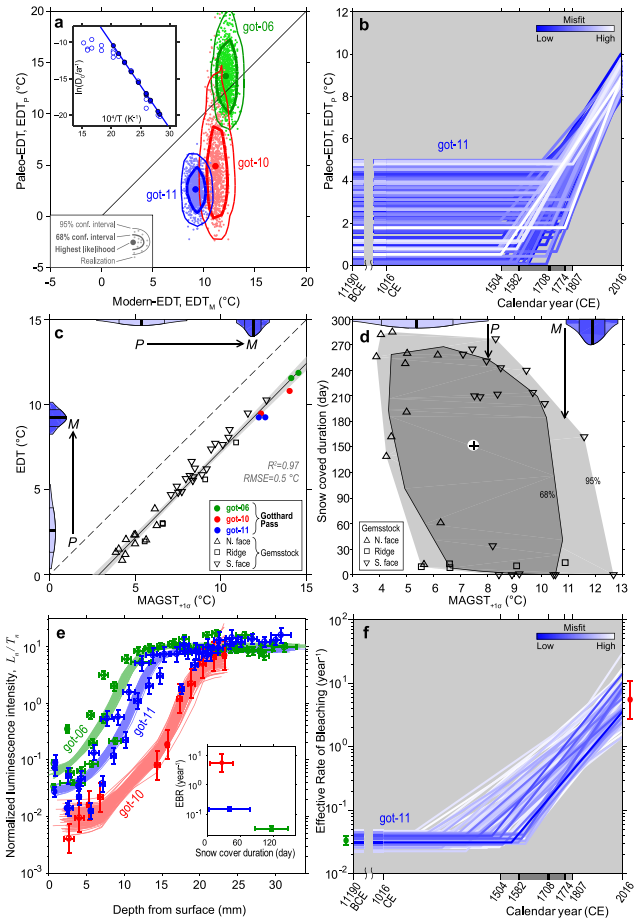

Figure 3. Interpretation of QHe (a–d) and IRSL (e, f) data. (a) Best-fit EDT_P versus estimated EDT_M for the three studied samples. Only for got-11 do these estimates statistically mismatch at 95% c.i., implying a remnant thermal history. Inset shows a single diffusion domain model (straight line) fitted to laboratory degassing experiments of proton-irradiated grains of got-11. (b) Inversion of got-11 ^{3}He data into a two-phase thermal history, where isothermal storage in the first phase is followed by a linear temperature increase toward its modern value (representative best-fit scenarios are shown). (c) Linear correlation between EDT and $MAGST_{+1\sigma}$ at a nearby modern analogue site (Gemsstock) enables the translation of paleo (P) and modern (M) EDT*s* at the Gotthard (*y*-axis) into corresponding $MAGST_{+1\sigma}$ (*x*-axis). The light and dark blue distributions along the *y*-axis correspond to $EDT_P = 2.6 \pm 2.6$°C and $EDT_M = 9.2 \pm 1.0$°C, respectively, implying a 6.6 ± 2.9°C increase (95% c.i.). (d) Snow cover duration versus $MAGST_{+1\sigma}$ at Gemsstock, with an underlying bagplot enveloping observable snowpack and temperature conditions. The transition from Paleo (P) to modern (M) conditions is discussed in text. (e) Spatial profiles of luminescence intensity versus rock depth (circles) and their best fitting models (curves) for the three studied samples; inset shows that the effective rate of bleaching (ERB) anticorrelates with modern snow cover duration (SCD). (f) Inversion of got-11 IRSL data into a two-phase isolation history (bounded by present-day insolation rates at got-06 and got-10), where constant bleaching rate in the first phase is followed by an exponential increase in bleaching rate toward its modern value in the second. Representative best-fit scenarios (colored paths) show that the onset of bleaching increase as recorded by IRSL overlaps with the onset of warming as recorded by QHe (cf. b); the magnitude of ERB increase is estimated at a factor ~10.

2. Methods and Results

2.1. QHe

The QHe method (Figure 1a) targets a specific product (^{3}He) of cosmic ray bombardment of near-surface rock quartz. Concurrently to its production, ^{3}He is also being continuously lost from quartz via thermally activated Arrhenius-type diffusion (Tremblay et al., 2014a). By accurately determining the diffusion kinetics (Figure 1c), alongside fixing the diffusion duration to an independent age control (e.g., ^{10}Be), it is possible to invert a measured cosmogenic ^{3}He into an effective thermal history (Tremblay et al., 2014a), namely the effective diffusion temperature (EDT). Being a weighted average, EDT is always shifted toward the peak temperature experienced (Tremblay et al., 2014a). From Figure 1e, it is evident that QHe is uniquely positioned to trace periglacial temperature fluctuations during the last millennia (Gribenski et al., 2022), as EDT of ~0°C corresponds to a mean lifetime of ~1,000 years (for representative kinetics of sample got-11).

Degassed natural ^{3}He from purified quartz separates (for got-06, -10, and -11) yielded QHe apparent exposure ages ranging from 0.8 to 2.5 ky (Figure 2d), up to an order of magnitude younger than their corresponding independent exposure age control (^{14}C-^{10}Be isochron; Hippe et al., 2014). The apparent ^{3}He age deficit was converted into an isothermal paleo-EDT (EDT_P) for each sample, with the uncertainty in EDT_P estimated by Monte Carlo simulation (Figure 3a shows 1,000 realizations per sample, further statistically aggregated). Concurrently, calculation of modern-EDT (EDT_M) using each site's modern thermometry data yielded isothermal EDT_M estimates (Figure 3a). Figure 3a demonstrates that the buttress of the glacial cirque (got-11) is the only site exhibiting a statistically significant QHe disequilibrium, with its EDT_M being significantly warmer (6.6 ± 2.9°C; 95% c.i.) than its corresponding EDT_P.

The quantified difference between EDT_P and EDT_M implies a recent change in the environmental temperature conditions, which the QHe system has still not fully equilibrated with. This mismatch can be further reconciled by allowing EDT_P to have varied with time toward its present-day estimate. To determine the timescale over which ground temperature could have increased at got-11, we modeled a two-phase thermal history spanning the ^{14}C-^{10}Be isochron age in which EDT_P is initially held constant, followed by a steady increase toward its modern value. A subset of all the successful inverse models that reproduce the observed ^{3}He at got-11 is shown in Figure 3b. Considering experimental uncertainties, the highest likelihood for the onset of ground surface temperature increase is constrained at 1708 CE, with its 95% confidence interval bracketing the onset of warming between 1504 and 1807 CE.

2.2. Modern Thermometry

Continuous, bi-hourly monitoring of near-surface ground surface temperature at sites got-06, -10, and -11 between summer 2016 and 2022 enables us to quantify modern annual snow cover duration (SCD, Figure 2f), the modern effective diffusion temperature EDT_M (Figure 3c), and the mean annual ground surface temperature (MAGST) summed with its 1 standard deviation, denoted as $MAGST_{+1\sigma}$ (Figure 2e). The latter is a compound variable, which was found to exhibit the highest correlation to EDT (Figure 3c). To complement these measurements with data from colder environments representative of got-11 prior to its inferred warming, we analyzed bi-hourly temperature

data from an additional 34 GST thermometers at the Gemsstock ridge (Haberkorn et al., 2015), located 6 km to the northeast, and ∼700 m higher (2,896–2,931 m asl) than the Gotthard Pass. The Gemsstock Ridge data set spans a broad range of microtopographic conditions and enables us to extend the linear relationship between EDT_M and $MAGST_{+1\sigma}$ from the Gotthard data (filled symbols in Figure 3c) down to freezing temperatures (open symbols in Figure 3b; $R^2 = 0.97$, RMSE = 0.5°C). The slope of the linear relationship between EDT_M and $MAGST_{+1\sigma}$ is indistinguishable from unity, implying that the same temperature increase (6.3 ± 2.3°C; 95% c.i.) applies to both. Thus, translation of EDT*s* into corresponding values of $MAGST_{+1\sigma}$ consists of a shift by −2.9 ± 0.5°C, allowing us to infer that at got-11, $MAGST_{+1\sigma}$ has evolved from 5.4 ± 2.6°C to 12.0 ± 1.0°C (95% c.i.).

Statistical analysis of the bivariate relationship (Rousseeuw et al., 1999; Verboven & Hubert, 2010) between present-day $MAGST_{+1\sigma}$ and SCD at the Gemsstock Ridge (Figure 3d) highlights two phenomena: (a) the colder north-facing (Δ) and warmer south-facing (∇) sites are unambiguously separated by a $MAGST_{+1\sigma}$ threshold at ∼6.5°C, and (b) the maximum attainable number of snow days is strongly anticorrelated with $MAGST_{+1\sigma}$, ranging from ∼280 days at ∼4°C to ∼160 days at ∼11.5°C. Extending this relationship onto the Gotthard data, we consider the conservative scenario of minimal warming at got-11, that is, transition from the highest EDT_P estimate to the lowest EDT_M estimate (marked "P→M" in Figures 3c and 3d). For this change, the 50% and 100% envelopes of observed SCD in Figure 3d reduce from ∼250 to ∼180 days, amounting to a cumulative loss of ∼70 days of annual snow. In a more likely scenario, the inferred $MAGST_{+1\sigma}$ change at got-11 from 5.4°C to 12.0°C could be commensurate with a 180° reversal of topographic aspect, where the median SCD of ∼150 days gradually became the upper achievable limit at present.

2.3. IRSL

The IRSL method (Figure 1b) quantifies an infrared-sensitive population of electrons trapped in lattice defects in feldspar. Exposure of these electrons to light results in their remobilization and recombination with holes, which is referred to as optical bleaching. At shallow rock depths, the bleaching rate is governed by a Beer-Lambert law (Sohbati, Jain, & Murray, 2012). By accurately determining the electron (de-)trapping kinetics (Figure 1d), alongside fixing the exposure duration to an independent age control, a luminescence depth profile can be inverted into an Effective Rate of Bleaching (ERB), which by analogy to EDT is a time-averaged metric of ground surface insolation intensity (Figure 1d). To obtain the paleo-ERB (ERB_P) at each study site, we measured the luminescence intensity of individual rock slices from vertically drilled cores (Sellwood et al., 2019), each ∼30 mm deep. At all sites, the normalized IRSL intensity increased with rock depth (Figure 3e), with the characteristic half-bleached depth $z_{1/2}$ ranging from 11.3 ± 0.3 mm (got-06) to 21.9 ± 1.6 mm (got-10). After a rigorous validation that the cumulative Holocene surface erosion is negligible with respect to the IRSL light attenuation length (Sohbati et al., 2018), and by utilizing an identical independent surface exposure age (Chapot et al., 2012) as used for the QHe inversion, the ERB_P at the three Gotthard Pass sites was constrained to $10^{-1.48\pm0.07}$ yr^{-1} at got-06, $10^{-0.82\pm0.09}$ yr^{-1} at got-11, and $10^{0.68\pm0.21}$ yr^{-1} at got-10, exhibiting as expected a strong anticorrelation with modern SCD (inset in Figure 3e).

To bracket the timing and magnitude of ERB_P change, we simulated the IRSL-depth profile of got-11 using a two-phase scenario, in which bleaching rate was kept constant in the first phase, and increased exponentially in the second. Due to the low bleaching rate, the modern ERB_M was not amenable to field calibration; therefore the ERB_M of got-11 was bracketed between the ERB_P values of got-06 and got-10 (marked outside the plot in Figure 3f), considered representative of snow-covered and -free conditions, respectively. Plausible fits of the observed IRSL-depth profile at got-11 were obtained solely by scenarios in which ERB_P increased with time (Figure 3f), consistent with a decrease in SCD (inset in Figure 3e). The highest likelihood of the onset of ERB_P increase occurs within the last millennium, broadly coinciding with the onset of EDT_P increase (cf. Figure 3b); we note that the lack of a direct independent estimate of a modern ERB_M renders the IRSL data set inversion as qualitative. Thus, our best estimate for the onset of the most recent environmental change (1708 CE), alongside its 68% and 95% confidence intervals (marked on the *x*-axes in Figures 3b and 3f) are based solely on the QHe data.

3. Discussion

The thermal regime of a rock surface is highly dependent on short- and longwave radiation, albedo, surface roughness, snow depth, and snow distribution in time and space. Nevertheless, investigations of the effects of

snow on thermal processes in steep rock walls are scarce (Haberkorn et al., 2015, 2017, 2021). With the absence of snowpack, GST of north facing slopes is highly correlated with air temperature, while a much lower correlation is seen on south facing slopes, with incoming solar radiation as a dominant driving factor of GST (Haberkorn et al., 2021). At rock wall locations with a thick snow cover, GST is strongly controlled by snow, since a sufficiently thick snowpack acts as a thermal insulator and decouples the rock surface from atmospheric influence (air temperature and solar radiation). Daily GST variations cease after the first large snowfalls, while GST oscillations are damped and lagged in time in comparison with air temperature (Haberkorn et al., 2017, 2021). Strong small-scale variability of up to 10°C in the distributed rock temperature data occurs within a few meters over the rock walls due to the variable snow distribution, revealing the heterogeneity and complexity of the thermal regime at a very local scale (Haberkorn et al., 2017). The fact that differences of up to 10°C in both MAGST and EDT may coexist across microtopography (10^1–10^2 m scales) characterized by a uniform mean annual air temperature (MAAT) (Haberkorn et al., 2021), emphasizes the uniqueness of the proposed tool to directly quantify bedrock response to climate change on a scale of an outcrop, thus significantly transcending the information currently accessible from either stable-isotope proxies (which reflect continentally-averaged MAAT; e.g., Dansgaard et al., 1993) or organic lipid proxies (whose dependence on MAAT is complicated by other factors; e.g., Peterse et al., 2012).

Our conservative estimate of a cumulative loss of ∼70 days of snow over a timescale of 330 ± 169 years (95% c.i.) is comparable both in magnitude and in timing to the SCD decline reconstructed from tree rings in Ventina valley, central Italian Alps, ∼100 km ESE of the Gotthard, at matching altitudes (Carrer et al., 2023). Furthermore, our timing for the onset of ground surface warming at the Gotthard is in line with an early end to a relatively weak Little Ice Age (LIA) in central Europe (Matthews & Briffa, 2005), in which 1700 CE marked the reversal of the long-term arctic cooling (Barboza et al., 2014; Kaufman et al., 2009; PAGES 2k Consortium, 2019). Locally, it is also in line with the complete absence of any LIA-aged landforms at the Gotthard Pass (Hippe et al., 2014). An estimate of a time-averaged SCD shortening rate at got-11 can be obtained by converting plausible EDT_P scenarios to a corresponding time-series of $MAGST_{+1\sigma}$ (Figure 3c), and further interpolating the latter onto the upper 68%–95% envelope of SCD (Figure 3d). The three-centuries averaged SCD shortening value of -0.38 ± 0.17 days yr^{-1} at got-11 (95% c.i.), is a factor 2 lower than its spatially closest modern estimate of -0.75 days yr^{-1} (regression of 1970–2015 monitoring data at Andermatt; Klein et al., 2016). The mismatch between modern and time-averaged SCD shortening rates strongly suggests that SCD decline at the Gotthard Pass must have proceeded in a nonlinear manner, with only the steepest and most recent trend captured by instrumental records. Although qualitative, the IRSL data suggests that the order-of-magnitude increase in ground insolation rate must have occurred during a comparable time window.

To evaluate our highest-likelihood environmental scenarios from QHe and IRSL data in the context of paleo-trends predicted by climate models (e.g., He & Clark, 2022), Figure 4 compares our estimates of EDT and ERB at got-11 to corresponding parameters from a 3 km × 3 km grid derived from CHELSA-TraCE21k (Karger et al., 2023). In terms of the timing of the onset of temperature rise and SCD drop, both QHe and IRSL data show good agreement with smoothed CHELSA-TraCE21k trends. Interestingly, both the EDT rise, and our inferred SCD decrease, are about a factor of 4 higher than those predicted by CHELSA-TraCE21k. This difference in magnitude is readily explained by two factors: (a) the temperature predictions in CHELSA-TraCE21k are for the mean and the diurnal temperature range of the near surface (2 m) air temperature (abbreviated $MANST_{+1\sigma}$), which, while correlated to $MAGST_{+1\sigma}$, exhibit smaller variance (see Supporting Information S1), and (b) the temperature and SCD predictions in CHELSA-TraCE21k contain a spatial averaging effect, since even within a single 1 km^2 cell containing got-11, there is significant variation in elevation, slope, and aspect. For example, the relative proportion of areas with similar slopes to that of got-11 (15–25°) is ∼25%. This explains why such a strong warming at got-11 (and similar sites) is damped at a coarser scale that averages over both flatter (e.g., such as got-06) as well as steeper areas (e.g., such as got-10) that might have experienced no snow change. In other words, strong local evidence of a multi-month decrease in snow cover in the last several hundred years, apparent in our proxy records of both MAGST and insolation at got-11, are diluted in comparatively coarser climate simulations, where microtopographic effects are averaged.

The presented novel pairing of cosmogenic (^{14}C, ^{10}Be, and ^{3}He) and luminescence (IRSL) techniques points to a tipping point transversal at got-11, where ∼150 SCD days likely became the upper limit of yearly snow accumulation at present. We believe that by quantifying both the timing and the magnitude of snowpack change in an Alpine environment over instrumentally inaccessible timescales, and by establishing a tipping point transversal

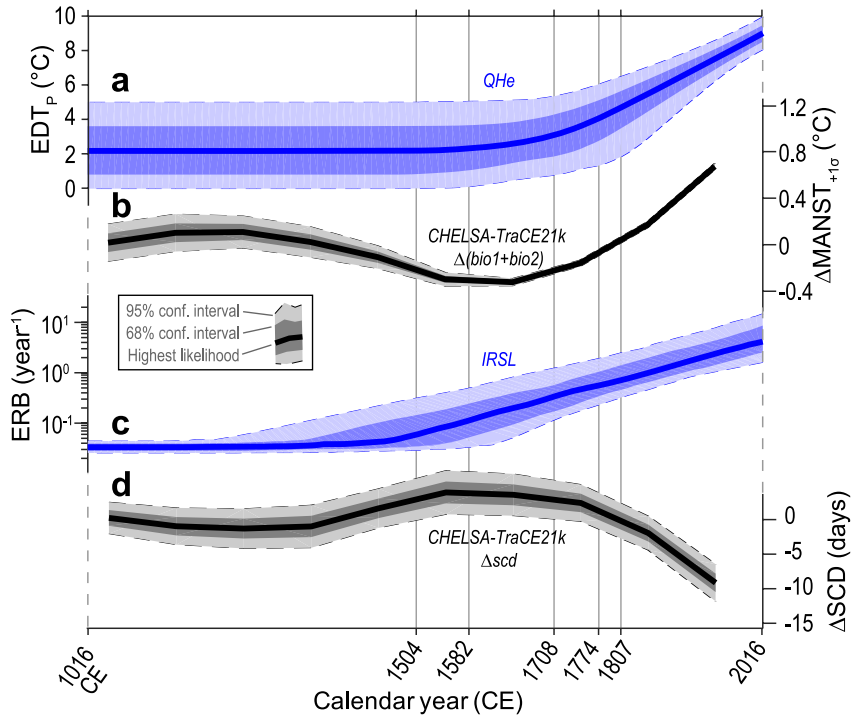

Figure 4. Comparison of our results to trends from the CHELSA-TraCE21k paleoclimate simulation (Karger et al., 2023), averaged over a 3 × 3 km^2 area (9 grid cells) centered at got-11 and relative to a datum at 1016 CE. (a) QHe-derived change in EDT$_p$ at got-11. (b) CHELSA-TraCE21k-derived relative change in sum of the Mean Annual Near Surface Temperature (CHELSA-TraCE21k parameter bio1) and its 1σ estimate (bio2). (c) ISRL-derived change in ERB at got-11. (d) CHELSA-TraCE21k-derived relative change in SCD. Note the overall agreement of all curves with respect to the onset of the latest environmental trend. The magnitude of EDT change (b) and inferred SCD at got-11 are a factor ∼4 higher than that in CHELSA-TraCE21k (a, d).

with respect to snowpack accumulation, our study sets a new climate reference point for a pre-industrialized snow-covered landscape in the Alps. In addition, we hope that it promotes the application of similar methodology in other localities, where detailed understanding of recent snow dynamics could be critical for accurate climate modeling and ultimately a more informed mitigation of the impacts of climate warming on mountain snowpack.

Data Availability Statement

All data and code used to generate the results and interpretations in this manuscript are published in Guralnik et al. (2023).

References

Ambühl, E. (1990). *Über Schneedecken in der Schweiz und Firne im Gotthardgebiet* (p. 428). Bern-Liebefeld. (unpublished manuscript, in German, deposited at the library of the Swiss Meteorological Institute, Zürich).

Arenson, L., Colgan, W., & Marshall, H. P. (2021). Physical, thermal, and mechanical properties of snow, ice, and permafrost. In *Snow and ice-related hazards, risks, and disasters* (pp. 35–71). Elsevier.

Barboza, L., Li, B., Tingley, M. P., & Viens, F. G. (2014). Reconstructing past temperatures from natural proxies and estimated climate forcings using short-and long-memory models. *Annals of Applied Statistics*, *8*(4), 1966–2001. https://doi.org/10.1214/14-aoas785

Bender, E., Lehning, M., & Fiddes, J. (2020). Changes in climatology, snow cover, and ground temperatures at high Alpine locations. *Frontiers in Earth Science*, *8*, 100. https://doi.org/10.3389/feart.2020.00100

Brunner, M. I., Götte, J., Schlemper, C., & Van Loon, A. F. (2023). Hydrological drought generation processes and severity are changing in the Alps. *Geophysical Research Letters*, *50*(2), e2022GL101776. https://doi.org/10.1029/2022gl101776

Buchmann, M., Begert, M., Brönnimann, S., & Marty, C. (2021). Local-scale variability of seasonal mean and extreme values of in situ snow depth and snowfall measurements. *The Cryosphere*, *15*(10), 4625–4636. https://doi.org/10.5194/tc-15-4625-2021

Carrer, M., Dibona, R., Prendin, A. L., & Brunetti, M. (2023). Recent waning snowpack in the Alps is unprecedented in the last six centuries. *Nature Climate Change*, *13*(2), 155–160. https://doi.org/10.1038/s41558-022-01575-3

Chapot, M. S., Sohbati, R., Murray, A. S., Pederson, J. L., & Rittenour, T. M. (2012). Constraining the age of rock art by dating a rockfall event using sediment and rock-surface luminescence dating techniques. *Quaternary Geochronology*, *13*, 18–25. https://doi.org/10.1016/j.quageo.2012.08.005

Acknowledgments
This research was funded by the Netherlands Organisation for Scientific Research (NWO) Veni Grant 863.15.026. MMT acknowledges support from the U.S. National Science Foundation (DGE-1106400) and the American Association for the Advancement of Science Marion Milligan Mason Award. D.L.S. acknowledges funding from the U.S. National Science Foundation (GEO-1322086) and the Anne and Gordon Getty Foundation. P.G.V. acknowledges funding from the French ANR-PIA program (ANR-18-MPGA-0006). The data from Gemmstock Ridge are part of PERMOS, the Swiss Permafrost Monitoring Network. BG thanks Christina Ankjærgaard and Tony Reimann for advice in obtaining the funding. We thank Hansueli Rhyner, Armin Dachauer, and Benjamin Lehmann for fieldwork assistance; Greg Balco for help with QHe measurements; Henning Loewe and Nora Helbig for discussions surrounding insolation; Dirk Scherler and Donovan Dennis for open dialogue regarding cosmogenic nuclide modelling; and Shan Ye, an anonymous reviewer, and Editor Sarah Feakins for constructive feedback.

Cicoira, A., Beutel, J., Faillettaz, J., & Vieli, A. (2019). Water controls the seasonal rhythm of rock glacier flow. *Earth and Planetary Science Letters*, *528*, 115844. https://doi.org/10.1016/j.epsl.2019.115844

Dansgaard, W., Johnsen, S. J., Clausen, H. B., Dahl-Jensen, D., Gundestrup, N. S., Hammer, C. U., et al. (1993). Evidence for general instability of past climate from a 250-Kyr ice-core record. *Nature*, *364*(6434), 218–220. https://doi.org/10.1038/364218a0

Davies, H. C., & Phillips, P. D. (1985). Mountain drag along the Gotthard section during ALPEX. *Journal of the Atmospheric Sciences*, *42*(20), 2093–2109. https://doi.org/10.1175/1520-0469(1985)042<2093:mdatgs>2.0.co;2

Gribenski, N., Tremblay, M. M., Valla, P. G., Balco, G., Guralnik, B., & Shuster, D. L. (2022). Cosmogenic ^{3}He paleothermometry on post-LGM glacial bedrock within the central European Alps. *Geochronology*, *4*(2), 641–663. https://doi.org/10.5194/gchron-4-641-2022

Guralnik, B., Tremblay, M. M., Phillips, M., Sellwood, E. L., Gribenski, N., Presl, R., et al. (2023). Data and code associated with the manuscript: Three centuries of snowpack decline at an Alpine pass revealed by cosmogenic paleothermometry and luminescence photochronometry (1.0) [Dataset]. Zenodo. https://doi.org/10.5281/zenodo.10050502

Haberkorn, A., Hoelzle, M., Phillips, M., & Kenner, R. (2015). Snow as a driving factor of rock surface temperatures in steep rough rock walls. *Cold Regions Science and Technology*, *118*, 64–75. https://doi.org/10.1016/j.coldregions.2015.06.013

Haberkorn, A., Kenner, R., Noetzli, J., & Phillips, M. (2021). Changes in ground temperature and dynamics in mountain permafrost in the Swiss Alps. *Frontiers in Earth Science*, *9*, 626686. https://doi.org/10.3389/feart.2021.626686

Haberkorn, A., Wever, N., Hoelzle, M., Phillips, M., Kenner, R., Bavay, M., & Lehning, M. (2017). Distributed snow and rock temperature modelling in steep rock walls using Alpine3D. *The Cryosphere*, *11*(1), 585–607. https://doi.org/10.5194/tc-11-585-2017

He, F., & Clark, P. U. (2022). Freshwater forcing of the Atlantic Meridional overturning circulation revisited. *Nature Climate Change*, *12*(5), 449–454. https://doi.org/10.1038/s41558-022-01328-2

Hippe, K., Ivy-Ochs, S., Kober, F., Zasadni, J., Wieler, R., Wacker, L., et al. (2014). Chronology of lateglacial ice flow reorganization and deglaciation in the Gotthard Pass area, Central Swiss Alps, based on cosmogenic ^{10}Be and in situ ^{14}C. *Quaternary Geochronology*, *19*, 14–26. https://doi.org/10.1016/j.quageo.2013.03.003

Karger, D. N., Nobis, M. P., Normand, S., Graham, C. H., & Zimmermann, N. E. (2023). CHELSA-TraCE21k–high-resolution (1 km) downscaled transient temperature and precipitation data since the Last Glacial Maximum. *Climate of the Past*, *19*(2), 439–456. https://doi.org/10.5194/cp-19-439-2023

Kaufman, D. S., Schneider, D. P., McKay, N. P., Ammann, C. M., Bradley, R. S., Briffa, K. R., et al. (2009). Recent warming reverses long-term Arctic cooling. *Science*, *325*(5945), 1236–1239. https://doi.org/10.1126/science.1173983

Kenner, R., Pruessner, L., Beutel, J., Limpach, P., & Phillips, M. (2020). How rock glacier hydrology, deformation velocities and ground temperatures interact: Examples from the Swiss Alps. *Permafrost and Periglacial Processes*, *31*(1), 3–14. https://doi.org/10.1002/ppp.2023

Klein, G., Vitasse, Y., Rixen, C., Marty, C., & Rebetez, M. (2016). Shorter snow cover duration since 1970 in the Swiss Alps due to earlier snowmelt more than to later snow onset. *Climate Change*, *139*(3–4), 637–649. https://doi.org/10.1007/s10584-016-1806-y

Li, Q., Yang, T., Zhang, F., Qi, Z., & Li, L. (2019). Snow depth reconstruction over last century: Trend and distribution in the Tianshan Mountains, China. *Global and Planetary Change*, *173*, 73–82. https://doi.org/10.1016/j.gloplacha.2018.12.008

Matthews, J. A., & Briffa, K. R. (2005). The "little ice age": Re-evaluation of an evolving concept. *Geografiska Annaler A*, *87*(1), 17–36. https://doi.org/10.1111/j.0435-3676.2005.00242.x

Mott, R., Scipión, D., Schneebeli, M., Dawes, N., Berne, A., & Lehning, M. (2014). Orographic effects on snow deposition patterns in mountainous terrain. *Journal of Geophysical Research: Atmospheres*, *119*(3), 1419–1439. https://doi.org/10.1002/2013jd019880

PAGES 2k Consortium. (2019). Consistent multi-decadal variability in global temperature reconstructions and simulations over the Common Era. *Nature Geoscience*, *12*(8), 643–649. https://doi.org/10.1038/s41561-019-0400-0

Peterse, F., van der Meer, J., Schouten, S., Weijers, J. W., Fierer, N., Jackson, R. B., et al. (2012). Revised calibration of the MBT–CBT paleotemperature proxy based on branched tetraether membrane lipids in surface soils. *Geochimica et Cosmochimica Acta*, *96*, 215–229. https://doi.org/10.1016/j.gca.2012.08.011

Rindt, O., Rosinger, C., Bonkowski, M., Rixen, C., Brüggemann, N., Urich, T., & Fiore-Donno, A. M. (2023). Biogeochemical dynamics during snowmelt and in summer in the Alps. *Biogeochemistry*, *162*(2), 257–266. https://doi.org/10.1007/s10533-022-01005-8

Rousseeuw, P. J., Ruts, I., & Tukey, J. W. (1999). The bagplot: A bivariate boxplot. *The American Statistician*, *53*(4), 382–387. https://doi.org/10.2307/2686061

Sellwood, E. L., Guralnik, B., Kook, M., Prasad, A. K., Sohbati, R., Hippe, K., et al. (2019). Optical bleaching front in bedrock revealed by spatially-resolved infrared photoluminescence. *Scientific Reports*, *9*(1), 2611. https://doi.org/10.1038/s41598-019-38815-0

Sohbati, R., Jain, M., & Murray, A. (2012). Surface exposure dating of non-terrestrial bodies using optically stimulated luminescence: A new method. *Icarus*, *221*(1), 160–166. https://doi.org/10.1016/j.icarus.2012.07.017

Sohbati, R., Liu, J., Jain, M., Murray, A., Egholm, D., Paris, R., & Guralnik, B. (2018). Centennial-to millennial-scale hard rock erosion rates deduced from luminescence-depth profiles. *Earth and Planetary Science Letters*, *493*, 218–230. https://doi.org/10.1016/j.epsl.2018.04.017

Tremblay, M. M., Shuster, D. L., & Balco, G. (2014a). Cosmogenic noble gas paleothermometry. *Earth and Planetary Science Letters*, *400*, 195–205. https://doi.org/10.1016/j.epsl.2014.05.040

Verboven, S., & Hubert, M. (2010). *Matlab library LIBRA* (Vol. 2, pp. 509–515). Wiley Inter. Rev.: Comput. Stat.

Watanabe, T., Suzuki, M., Komoto, Y., Shirai, K., & Yamazaki, A. (2021). Daily and annual shell growth in a long-lived freshwater bivalve as a proxy for winter snowpack. *Palaeogeography, Palaeoclimatology, Palaeoecology*, *569*, 110346. https://doi.org/10.1016/j.palaeo.2021.110346

Woodhouse, C. A. (2003). A 431-yr reconstruction of western Colorado snowpack from tree rings. *Journal of Climate*, *16*(10), 1551–1561. https://doi.org/10.1175/1520-0442-16.10.1551

References From the Supporting Information

Andričević, P., Sellwood, E. L., Eppes, M. C., Kook, M., & Jain, M. (2023). Passive atomic-scale optical sensors for mapping light flux in ultrasmall cavities. *Scientific Reports*, *13*(1), 5309. https://doi.org/10.1038/s41598-023-32010-y

Auclair, M., Lamothe, M., & Huot, S. (2003). Measurement of anomalous fading for feldspar IRSL using SAR. *Radiation Measurements*, *37*(4–5), 487–492. https://doi.org/10.1016/s1350-4487(03)00018-0

Balco, G., Stone, J. O., Lifton, N. A., & Dunai, T. J. (2008). A complete and easily accessible means of calculating surface exposure ages or erosion rates from ^{10}Be and ^{26}Al measurements. *Quaternary Geochronology*, *3*, 174–195. https://doi.org/10.1016/j.quageo.2007.12.001

Berger, A., Herwegh, M., Schwarz, J.-O., & Putlitz, B. (2011). Quantitative analysis of crystal/grain sizes and their distributions in 2D and 3D. *Journal of Structural Geology*, *33*(12), 1751–1763. https://doi.org/10.1016/j.jsg.2011.07.002

Boeckli, L., Brenning, A., Gruber, S., & Noetzli, J. (2012). Permafrost distribution in the European Alps: Calculation and evaluation of an index map and summary statistics. *The Cryosphere*, *6*(4), 807–820. https://doi.org/10.5194/tc-6-807-2012

Braun, J., Van der Beek, P., & Batt, G. (2006). *Quantitative thermochronology: Numerical methods for the interpretation of thermochronological data*. Cambridge University Press.

Choi, J. H., Duller, G. A. T., & Wintle, A. G. (2006). Analysis of quartz LM-OSL curves. *Ancient TL*, *24*, 9–20.

Dąbski, M. (2012). Determining rock surface micro-roughness and search for new method of relative dating of glacial landforms: A case study from Fláajökull (SE Iceland) and Biferten glacier (Swiss Alps) forefields. *Landform Analysis*, *21*, 3–8.

Dennis, D. P., & Scherler, D. A. (2022). Combined cosmogenic nuclides approach for determining the temperature-dependence of erosion. *Journal of Geophysical Research: Earth Surface*, *127*(4), e2021JF006580. https://doi.org/10.1029/2021jf006580

Devroye, L. (1986). Sample-based non-uniform random variate generation. In *In Proceedings of the 18th conference on winter simulation* (pp. 260–265).

Elkadi, J., Lehmann, B., King, G. E., Steinemann, O., Ivy-Ochs, S., Christl, M., & Herman, F. (2022). Quantification of post-glacier bedrock surface erosion in the European Alps using ^{10}Be and optically stimulated luminescence exposure dating. *Earth Surface Dynamics*, *10*(5), 909–928. https://doi.org/10.5194/esurf-10-909-2022

Fechtig, H., & Kalbitzer, S. (1966). The diffusion of argon in potassium bearing solids. In O. A. Schaeffer & J. Zahringer (Eds.), *Potassium—Argon dating* (pp. 68–106). Springer.

Freiesleben, T. H., Thomsen, K. J., & Jain, M. (2023). Novel luminescence kinetic models for rock surface exposure dating. *Radiation Measurements*, *160*, 106877. https://doi.org/10.1016/j.radmeas.2022.106877

Guralnik, B., & Sohbati, R. (2019). Fundamentals of luminescence photo-and thermochronometry. In *Advances in physics and applications of optically and thermally stimulated luminescence* (pp. 399–437).

Kabacińska, Z., Timar-Gabor, A., & Guralnik, B. (2021). Meyer-Neldel rule on thermal stability parameters (trap depth and frequency factor) of luminescence signals in quartz. In *In EGU general assembly conference abstracts (EGU21-10775)*.

Kenner, R., Noetzli, J., Hoelzle, M., Raetzo, H., & Phillips, M. (2019). Distinguishing ice-rich and ice-poor permafrost to map ground temperatures and ground ice occurrence in the Swiss Alps. *The Cryosphere*, *13*(7), 1925–1941. https://doi.org/10.5194/tc-13-1925-2019

Lilliefors, H. W. (1967). On the Kolmogorov-Smirnov test for normality with mean and variance unknown. *Journal of the American Statistical Association*, *62*(318), 399–402. https://doi.org/10.1080/01621459.1967.10482916

Liu, L., & Guo, Q. X. (2001). Isokinetic relationship, isoequilibrium relationship, and enthalpy-entropy compensation. *Chemistry Review*, *101*(3), 673–696. https://doi.org/10.1021/cr990416z

Lopez-Sanchez, M. A. (2018). GrainSizeTools: A Python script for grain size analysis and paleopiezolmetry based on grain size. *Journal of Open Source Software*, *3*, 863.

Lopez-Sanchez, M. A., & Llana-Fúnez, S. (2016). An extension of the Saltykov method to quantify 3D grain size distributions in mylonites. *Journal of Structural Geology*, *93*, 149–161. https://doi.org/10.1016/j.jsg.2016.10.008

Nunes, R. V., & Swartzel, K. R. (1990). Modeling chemical and biochemical changes under sinusoidal temperature fluctuations. *Journal of Food Engineering*, *11*(2), 119–132. https://doi.org/10.1016/0260-8774(90)90048-d

Polymeris, G. S., Sfampa, I., Niora, M., Stefanaki, E., Malletzidou, L., Giannoulatou, V., et al. (2018). Anomalous fading in TL, OSL and TA–OSL signals of Durango apatite for various grain size fractions; from micro to nano scale. *Journal of Luminescence*, *195*, 216–224. https://doi.org/10.1016/j.jlumin.2017.11.034

Roberts, H. M., & Duller, G. A. (2004). Standardised growth curves for optical dating of sediment using multiple-grain aliquots. *Radiation Measurements*, *38*(2), 241–252. https://doi.org/10.1016/j.radmeas.2003.10.001

Saltykov, S. A. (1967). The determination of the size distribution of particles in an opaque material from a measurment of the size distribution of their sections. In H. Elias (Ed.), *Proceedings of the second international congress for stereology* (pp. 163–173). Springer Berlin Heidelberg.

Savi, S., Delunel, R., & Schlunegger, F. (2015). Efficiency of frost-cracking processes through space and time: An example from the eastern Italian Alps. *Geomorphology*, *232*, 248–260. https://doi.org/10.1016/j.geomorph.2015.01.009

Scheil, E. (1931). Die Berechnung der Anzahl und Großenverteilung kugelförmiger Kristalle in undurchsichtigen Körpern mit Hilfe der durch einen ebenen Schnitt erhaltenen Schnittkreise. *Zeitschrift für Anorganische und Allgemeine Chemie*, *201*(1), 259–264. https://doi.org/10.1002/zaac.19312010123

Schneider, C., Rasband, W., & Eliceiri, K. (2012). NIH image to ImageJ: 25 years of image analysis. *Nature Methods*, *9*(7), 671–675. https://doi.org/10.1038/nmeth.2089

Schwartz, H. A. (1934). The metallographic determination of the size distribution of temper carbon nodules. *Metals Alloys*, *5*, 139.

Shuster, D. L., & Farley, K. A. (2005). Diffusion kinetics of proton-induced ^{21}Ne, ^{3}He, and ^{4}He in quartz. *Geochimica et Cosmochimica Acta*, *69*(9), 2349–2359. https://doi.org/10.1016/j.gca.2004.11.002

Sohbati, R., Murray, A. S., Chapot, M. S., Jain, M., & Pederson, J. (2012). Optically stimulated luminescence (OSL) as a chronometer for surface exposure dating. *Journal of Geophysical Research*, *117*(B9), 1–7. https://doi.org/10.1029/2012jb009383

Sohbati, R., Murray, A. S., Jain, M., Buylaert, J. P., & Thomsen, K. J. (2011). Investigating the resetting of OSL signals in rock surfaces. *Geochronometria*, *38*(3), 249–258. https://doi.org/10.2478/s13386-011-0029-2

Stoica, P., & Selen, Y. (2004). Model-order selection: A review of information criterion rules. *IEEE Signal Processing Magazine*, *21*(4), 36–47. https://doi.org/10.1109/msp.2004.1311138

Tatone, B. S. A., & Grasselli, G. (2009). Use of a stereo-topometric measurement system for the characterization of rock joint roughness in-situ and in the laboratory. In *Proceedings of the 3rd CANUS rock mechanics symposium*. (pp. 1–14).

The MathWorks Inc. (2022). MATLAB version: 9.2.0 (R2017a), *Natick, Massachusetts*. Retrieved from https://www.mathworks.com

Tremblay, M. M., Shuster, D. L., & Balco, G. (2014b). Diffusion kinetics of ^{3}He and ^{21}Ne in quartz and implications for cosmogenic noble gas paleothermometry. *Geochimica et Cosmochimica Acta*, *142*, 186–204. https://doi.org/10.1016/j.gca.2014.08.010

Tremblay, M. M., Shuster, D. L., Spagnolo, M., Renssen, H., & Ribolini, A. (2019). Temperatures recorded by cosmogenic noble gases since the last glacial maximum in the Maritime Alps. *Quaternary Research*, *91*(2), 829–847. https://doi.org/10.1017/qua.2018.109

Trull, T. W., Kurz, M. D., & Jenkins, W. J. (1991). Diffusion of cosmogenic ^{3}He in olivine and quartz: Implications for surface exposure dating. *Earth and Planetary Science Letters*, *103*(1–4), 241–256. https://doi.org/10.1016/0012-821x(91)90164-d

Vermeesch, P., Baur, H., Heber, V. S., Kober, F., Oberholzer, P., Schaefer, J. M., et al. (2009). Cosmogenic ^{3}He and ^{21}Ne measured in quartz targets after one year of exposure in the Swiss Alps. *Earth and Planetary Science Letters*, *284*(3–4), 417–425. https://doi.org/10.1016/j.epsl.2009.05.007

Wang, D., Chen, X., Oeser, M., Stanjek, H., & Steinauer, B. (2014). Study of micro-texture and skid resistance change of granite slabs during the polishing with the Aachen Polishing Machine. *Wear*, *318*(1–2), 1–11. https://doi.org/10.1016/j.wear.2014.06.005

Wolf, R. A., Farley, K. A., & Kass, D. M. (1998). Modeling of the temperature sensitivity of the apatite (U–Th)/He thermochronometer. *Chemical Geology*, *148*(1–2), 105–114. https://doi.org/10.1016/s0009-2541(98)00024-2